

A Model for Type-IIP Supernovae with Medium Recombination Approximation

HONG-XUAN JIANG^{1,2,*} AND XUE-WEN LIU²

¹*Tsung-Dao Lee Institute, Shanghai Jiao Tong University, Shengrong Road 520, Shanghai, 201210, People's Republic of China*

²*College of Physics, Sichuan University, Chengdu, 610065, People's Republic of China*

Submitted to ApJ

ABSTRACT

In this paper, we propose a new light-curve model for Type-IIP supernovae (SNe IIP) with an approximation of medium recombination. Recombination of hydrogen that takes place in the envelope is believed highly affect the light curves of SNe IIP. The propagation of the recombination wave through the expanding envelope is crucial to determine the temperature and the bolometric luminosity. Several approximations were made in previous works to determine the recombination front, which plays a role as the pseudo-photosphere. With the Eddington boundary condition, we let the actual photosphere be the boundary to determine the time evolution of temperature profile of the envelope and calculate the bolometric luminosity. A new approximation on the speed of recombination wave is introduced to get a closer result to the real situation. We abandon the non-self-consistent approximations made in former works and solve the initial hump problem in the previous attempt for the slow recombination approximation. The produced light curves show the necessity of this approximation and fit the observation well.

Keywords: Type IIP supernovae, photosphere, recombination wave

1. INTRODUCTION

Type II and a subset of Type I (Ib/Ic; stripped envelope) supernovae are widely accepted to be originated from the core collapse of stars with zero-age-main-sequence mass of $\geq 8 M_{\odot}$ (Smartt 2015). SNe II are defined by the presence of hydrogen in their spectra and classified according to their shape of light curves: Type IIL with a linearly declining light curve, whereas Type IIP displaying an extended plateau lasting ~ 100 days. Despite some authors find growing evidence that SNe II form a continuum of light-curve properties, the separation between SNe IIP and IIL is still an open issue (Arcavi 2012; Faran 2014; Anderson 2014; Sanders 2015; Valenti et al. 2016; Galbany et al. 2016; Rubin et al. 2016; Hillier 2019). Kou (2020) found that the profile of the H_{α} spectral line may be the key to distinguishing the two types of SNe II. However, it is still an open question.

Indeed, the amount and distribution of hydrogen is one of the most important ingredients in shaping the long-lasting optical plateau of SNe II through recombination effect (Grassberg 1971; Falk&Arnett 1973; Arnett & Fu 1989; Popov 1993; Kasen&Woosley 2009; Dessart 2013; Nagy et al. 2014; Faran 2019). The spatial distribution of ^{56}Ni also plays an important role in extending and flattening the plateau of the light curves (Nakar 2016; Kozyreva 2019). One-dimensional (1D) radiation hydrodynamical code STELLAR or radiation transport code Sedona based on 1D progenitor model MESA including the above effects can synthesize the light curves of SNe IIP (Paxton 2018, 2019; Goldberg 2019; Kasen&Woosley 2009; Ricks 2019). Three-dimensional neutrino-driven explosion simulations can now explain the basic observational data of ordinary SNe IIP (Utrobin 2017). However, a simple analytical method without complicated, time-consuming simulations is still useful to obtain the basic physical parameters such as explosion energy, ejected mass and initial radius for the first order-approximation. Moreover, the analytical scalings between the parameters have a clear

Corresponding author: Xue-Wen Liu
liuxuew@scu.edu.cn

* hongxuan.jiang@sjtu.edu.cn

physical explanation and are easily compared with the observations.

An analytical model for SNe was proposed by Arnett which described the light curve properties of SNe I and SNe II in detail (Arnett 1980, 1982; Arnett & Fu 1989). With the help of Arnett’s model, some important parameters, e.g., ejecta mass, explosion energy, and initial radius can be estimated quickly (Nagy et al. 2014). Arnett & Fu (1989) discussed the effects of ionization on the light curves of SNe II under the approximation of fast recombination. Two approximations about the speed of hydrogen recombination in SNe IIP are summarized in Arnett (1996), in which slow recombination approximation was introduced. For the fast recombination model, the temperature profile remains unchanged when the recombination front recedes through the envelope. While the slow approximation assumes the temperature profile of the envelope evolves strictly with the recession of the recombination front (Arnett 1996). Based on the fast recombination approximation, Nagy et al. (2014) successfully produced the light curves of SNe IIP and fitted observations very well. Although their model can not explain the cusp of the light curves of SNe IIP at very early epochs, their model demonstrates the effect of recombination is the critical factor in the formation of the light curves of SNe IIP. In the following paper, they solved the cusp problem by using a two-component model (Nagy & Vinkó 2016).

The main difference between the fast and slow approximations is the boundary condition of the spatial equation of the model. The fast approximation is widely assumed in previous works (see Nagy et al. (2014); Zampieri et al. (2003); Chatzopoulos et al. (2012)). The boundary is simply set to be the outmost edge of the hydrogen-rich envelope. However, the slow approximation requires calculating the real-time temperature profile of the envelope. Thus time-dependent boundary is required. In Arnett (1980), the Eddington surface boundary condition was introduced, giving constraints on the spatial temperature profile ψ at the photosphere (Eddington 1926). Assuming the receding recombination front as the pseudo-photosphere, Arnett & Fu (1989) implied that the eigenvalue α of the temperature profile increases in proportion to $1/x_i^2$, where x_i is the dimensionless radius of the recombination front. Arnett (1996) implemented this idea to the calculation of light curve. However, the produced light curve has a big bump at the end of the plateau phase, which is not physical. Using the ”radiative-zero” boundary condition (Arnett 1980), Popov (1993) assumed the temperature at the recombination front is zero and pointed out the necessity of time-dependent radial temperature

profile. His result is also consistent with the relation of $\alpha(t) \propto 1/x_i^2(t)$. α is the eigenvalue for the spatial equation, which describe the shape of the radial temperature profile. However, the zero surface temperature assumption is too rough to strictly fit observation. More detailed model is required.

Recently, Liu et al. (2018) considered the recession of the real photosphere and derived its radius evolution, which is consistent with observed supernova-like explosion. Jiang et al. (2022) then propose a method to obtain the light curve when the photosphere recession effect is presented. In this paper, we further add the recombination effect to construct a semi-analytical light curve model for SNe IIP. We can remove the approximations made in Arnett & Fu (1989), which result in the bump during the plateau phase. We adopt a boundary condition on the recession photosphere to determine the instantaneous temperature profile, which leads to the coevolution of α and x_{ph} . The SN ejecta is homologous, spherically symmetric and the density profile is exponential or uniform. The opacity is assumed to be a simple step-function of temperature introduced in Arnett & Fu (1989).

This paper is organized as follows. In Section 2, we describe the model. In Section 3, we describe the medium recombination approximation in detail. In Section 4, we compare our model with previous models. In Section 5, we discuss the effects of each parameter. In Section 6, we describe the shell component in our model. In Section 7, we fit 5 well studied sources. Finally, in Section 8, we give our conclusion.

2. MODEL CONSTRUCTION AND APPROXIMATIONS

2.1. The light curve model

Based on the model of Arnett (1980), Arnett & Fu (1989) added the recombination effect. In this section, we modify some of their assumptions and consider the effect of photosphere recession and thus time-dependent boundary.

Taking the same separation of variables in Arnett (1980), we can separate the temporal and spatial part of temperature as follows

$$T^4(x, t) = T^4(0, 0)\psi(x)\phi(t) \left(\frac{R_0}{R(t)} \right)^4, \quad (1)$$

where $\psi(x)$ and $\phi(t)$ are the spatial and temporal profiles, respectively. Since the ejecta is homologous, we define x to be a dimensionless variable which satisfies $x = r/R(t)$. In the same way, the density profile can

also be separated as follows

$$\rho(x, t) = \rho_0 \eta(x) \left(\frac{R_0}{R(t)} \right)^3, \quad (2)$$

where $\eta(x)$ is the spatial distribution.

In the diffusion approximation, the luminosity L is

$$\frac{L}{4\pi r^2} = -\frac{\lambda c}{3} \frac{\partial aT^4}{\partial r}, \quad (3)$$

where $\lambda = 1/\rho\kappa$ is the mean free path, κ is opacity, and a is the Stefan–Boltzmann constant.

We assume the extra energy source is the release of nuclear energy by ^{56}Ni decay only (which is also the assumption in Arnett (1982)). The nickel ^{56}Ni turns into ^{56}Co through radioactive decay. The decay of ^{56}Ni and ^{56}Co provides the energy source for SNe II and forms a radioactive tail in the light curves (Barbon et al. 1984). The abundance equations can be written as

$$\frac{dX_{\text{Ni}}(t)}{dt} = -\frac{X_{\text{Ni}}(t)}{\tau_{\text{Ni}}}, \quad (4)$$

$$\frac{dX_{\text{Co}}(t)}{dt} = \frac{X_{\text{Ni}}(t)}{\tau_{\text{Ni}}} - \frac{X_{\text{Co}}(t)}{\tau_{\text{Co}}}, \quad (5)$$

where τ_{Ni} and τ_{Co} are the decay time of ^{56}Ni and ^{56}Co respectively. As defined in Arnett (1982), the expression of the energy release ϵ can be written as

$$\epsilon = \epsilon_{\text{Ni}} M_{\text{Ni}} \zeta(t), \quad (6)$$

where

$$\zeta(t) = X_{\text{Ni}}(t) + \frac{\epsilon_{\text{Co}}}{\epsilon_{\text{Ni}}} X_{\text{Co}}(t). \quad (7)$$

ϵ_{Ni} and ϵ_{Co} are the energy production rate via radioactive decay.

Note that the first law of thermodynamics can be written as

$$\frac{dE}{dt} + P \frac{dV}{dt} = \epsilon - \frac{\partial L}{\partial m}, \quad (8)$$

where E is thermal energy per unit mass, P is pressure and $V = 1/\rho$. For radiation gas, we have energy density $E = aT^4 V$ and pressure $P = aT^4/3$.

The temperature of the hydrogen-rich envelope of SNe II is more than 10^6 K at the very beginning, which means the whole envelope is fully ionized. As the envelope expands outwards, the temperature cools down gradually. Adopting the same assumption in Arnett & Fu (1989), when the temperature is lower than recombination temperature T_{ion} , the local opacity is zero. For the plasma with temperature higher than T_{ion} , its opacity is a constant κ_t . Therefore a recombination front x_i divides the envelope into two parts, and the opacity function can be written as

$$\kappa(T) = \begin{cases} \kappa_t, & T > T_{\text{ion}} \\ 0, & T < T_{\text{ion}} \end{cases}. \quad (9)$$

As the same in Arnett (1980) and Liu et al. (2018), we also choose optical depth $q = 2/3$ to determine the photosphere x_{ph} . This value comes from the approximation of a plane-parallel atmosphere. Using the equation in Liu et al. (2018)

$$\int_{r_{\text{ph}}}^{r_i} \rho(x, t) \kappa_t dr = 2/3, \quad (10)$$

where r_i is the radius of the recombination front. For the rest of calculation, we assume an exponential density distribution

$$\eta(x) = e^{Ax}. \quad (11)$$

Substituting $\rho(x, t)$ into Eq. (10), we obtain the expression of x_{ph} (Jiang et al. 2022):

$$x_{\text{ph}} = \frac{1}{A} \ln \left[e^{Ax_i} - A \frac{2R^2(t)}{3R_0^3 \kappa_t} \right], \quad (12)$$

where x_i is dimensionless radius of the recombination front, i.e. $T(x_i) = T_{\text{ion}}$.

Photons that reach the photosphere can escape freely. Therefore the contribution outside of the photosphere is neglected. Using the first law of thermodynamics, we have

$$\dot{E}_{\text{ph}} + (P\dot{V})_{\text{ph}} = \epsilon_{\text{ph}} - L_{\text{ph}}. \quad (13)$$

Define

$$\begin{aligned} E_{\text{ph}} &= \int_0^{r_{\text{ph}}} aT^4 4\pi r^2 dx \\ &= E_{\text{Th}}^0 \frac{I_{\text{ph}}}{I_{\text{Th}}^0} \frac{R_0}{R(t)} \phi(t), \end{aligned} \quad (14)$$

where $E_{\text{Th}}^0 = 4\pi R_0^3 aT_0^4 I_{\text{Th}}^0$ is the initial thermal energy of the envelope, $I_{\text{ph}} = \int_0^{x_{\text{ph}}} \psi(x) x^2 dx$ and $I_{\text{Th}}^0 = \int_0^1 \psi^0(x) x^2 dx$ are the integration of the radial profile. $\psi^0(x)$ is the initial radial temperature profile, while $\psi(x)$ varies with the recession of photosphere. Thus the time derivative of it is written as

$$\begin{aligned} \dot{E}_{\text{ph}} &= E_{\text{ph}} \left(\frac{\dot{\phi}}{\phi} - \frac{v_{\text{sc}}}{R(t)} + \frac{\dot{I}_{\text{ph}}}{I_{\text{ph}}} \right) \\ &= E_{\text{ph}} \left(\frac{d \ln \phi}{dt} - \frac{d \ln R}{dt} + \frac{d \ln I_{\text{ph}}}{dt} \right). \end{aligned} \quad (15)$$

Note that as in Arnett & Fu (1989):

$$\frac{d \ln V}{dt} = 3 \frac{d \ln R}{dt}, \quad (16)$$

and pressure $P = aT^4/3$, we rearrange Eq. (15) as follows

$$\dot{E}_{\text{ph}} + E_{\text{ph}} \frac{d \ln R}{dt} = E_{\text{ph}} \left(\frac{\dot{\phi}}{\phi} + \frac{\dot{I}_{\text{ph}}}{I_{\text{ph}}} \right), \quad (17)$$

which is exactly the left side of Eq. (13). Substitute Eq. (17) into the L.H.S of Eq. (13), we obtain

$$\dot{E}_{\text{ph}} + (P\dot{V})_{\text{ph}} = E_{\text{ph}} \left(\frac{\dot{\phi}}{\phi} + \frac{\dot{I}_{\text{ph}}}{I_{\text{ph}}} \right), \quad (18)$$

where the time derivative of I_{ph} is written as

$$\dot{I}_{\text{ph}} = \psi(x_{\text{ph}})x_{\text{ph}}^2 \dot{x}_{\text{ph}} \quad (19)$$

Substituting Eq. (1) into Eq. (3) we obtain:

$$\begin{aligned} L(x, t) &= -\frac{4\pi a T^4(0, 0) c R_0}{3\rho_0 \kappa_t} \phi(t) \frac{x^2}{\eta(x)} \frac{d\psi(x)}{dx} \\ &= -\frac{E_{\text{Th}}^0}{\tau_d I_{\text{Th}}^0 \alpha} \phi(t) \frac{x^2}{\eta(x)} \frac{d\psi(x)}{dx}, \end{aligned} \quad (20)$$

where

$$\tau_d = \frac{3\rho_0 \kappa_t R_0^2}{\alpha c}$$

Thus combining luminosity term Eq. (20), radioactive decay term Eq. (6) and Eq. (18), we can obtain a partial differential equation. Using the widely used technique in (Arnett 1980, 1982; Arnett & Fu 1989), this equation can be separated into temporal and spatial parts, which are shown as follows.

Spatial part:

$$\frac{1}{\psi(x)x^2} \frac{d}{dx} \left(\frac{x^2}{\eta(x)} \frac{d\psi}{dx} \right) = -\alpha, \quad (21)$$

where α is the eigenvalue. As our previous work (see Jiang et al. (2022)) suggests, α varies with the recession of photosphere.

Substituting the definition of I_{ph} into Eq: (21), the complicated spatial term in Eq. (20) can be replaced with a simple I_{ph} .

$$\begin{aligned} \frac{x^2}{\eta(x)} \frac{d\psi}{dx} &= -\alpha \int \psi(x)x^2 dx \\ &= -\alpha I_{\text{ph}}. \end{aligned} \quad (22)$$

And the luminosity can be simplified as

$$L(x, t) = \frac{E_{\text{Th}}^0}{\tau_d} \frac{I_{\text{ph}}}{I_{\text{Th}}^0} \phi(t). \quad (23)$$

After some algebra, the temporal part is obtained

$$\frac{d\phi(t)}{dt} = \frac{R(t)}{R_0} \left[p_1 \frac{I_{\text{Th}}^0}{I_{\text{ph}}} \zeta(t) - \frac{\phi(t)}{\tau_d} \right] - \phi(t) \frac{\psi(x_{\text{ph}})x_{\text{ph}}^2}{I_{\text{ph}}} \frac{dx_{\text{ph}}}{dt}, \quad (24)$$

where $p_1 = \epsilon_{\text{Ni}} M_{\text{Ni}}^0 / E_{\text{Th}}^0$.

Finally, the effects of gamma-ray leakage and recombination heat from Hydrogen can be added to the luminosity as

$$L(t) = \frac{E_{\text{Th}}^0}{\tau_d} \frac{I_{\text{ph}}}{I_{\text{Th}}^0} \phi(t) \left(1 - e^{A_g/t^2} \right) + 4\pi^2 r_i^2 Q \rho(x_i, t) \frac{dr_i}{dt}, \quad (25)$$

where A_g is the effectiveness of gamma-ray trapping, and $Q = 1.6 \times 10^{13} (Z/A) Z^{4/3}$ is the recombination energy per unit mass. A_g is significant in modeling the light curves of Type IIb and Ib/c SNe (Nagy et al. 2014). The optical depth of gamma-rays can be defined as $\tau_g = A_g/t^2$ (Nagy et al. 2014; Chatzopoulos et al. 2012).

2.2. Assumptions made by Arnett & Fu (1989)

Two assumptions were made in Arnett & Fu (1989) to separate the variables. For the spatial of the temperature profile, they assumed shape invariance of $\psi(x)$

$$\int_0^{x_i} \psi(x)x^2 dx = x_i^3 \int_0^1 \psi(x)x^2 dx = x_i^3 I_{\text{Th}}^0, \quad (26)$$

and

$$\left. \frac{d\psi(x)}{dx} \right|_{x=x_i} = -\frac{1}{x_i}. \quad (27)$$

In most cases, it is not true to simply assuming $\psi(x) \propto \ln \frac{1}{x}$ as in Eq. (27). Letting the recombination front to be the pseudo-photosphere (Arnett & Fu 1989; Nagy et al. 2014), then Eq. (26) gives $I_{\text{ph}} = x_{\text{ph}}^3 I_{\text{Th}}^0$. Taking the uniform density case as an example, we have $\psi(x) = \sin(\pi x)/\pi x$ in this case. $I_{\text{ph}} \approx x_{\text{ph}}^3 I_{\text{Th}}^0$ is valid only when x tends to zero. In other cases, such approximation may lead to an incorrect result. In our model, we abandon these approximations and calculate the L.H.S of Eq. (26) and (27) numerically to avoid this problem.

2.3. The receding boundary condition

In the literature, fixed boundary condition is assumed (fast recombination approximation). As discussed in Arnett (1980), it is only valid for dense objects. When the envelope expands, the density of the outer layer decreases rapidly. Then such an assumption might not be appropriate. If the relaxation time of the radial temperature profile of the envelope is short enough, Eddington's boundary condition is needed:

$$acT^4 = \frac{3}{4} T_e^4 (\tau + q). \quad (28)$$

If we take $q = 1$, the Eddington approximation can be written as

$$\frac{\partial \psi}{\partial x} = -\frac{3}{4} \psi_e \frac{R(t)}{\lambda(x)}. \quad (29)$$

So at the photosphere

$$\psi(x_{\text{ph}}) = -\frac{4}{3} \frac{\lambda(x_{\text{ph}})}{R(t)} \frac{\partial \psi(x)}{\partial x} \Big|_{x=x_{\text{ph}}}. \quad (30)$$

The expression of $\psi(x)$ can be obtained by solving Eq. (21). Unfortunately it is only analytically solvable when the density distribution is uniform, i.e., $\eta(x) = 1$. In this case $\psi(x) = \sin(\sqrt{\alpha}x)/\sqrt{\alpha}x$. If the density is an exponential distribution, i.e., $\eta(x) = e^{Ax}$. Eq. (21) can only be solved numerically. The solution of Eq. (21) contains an unknown parameter α , which is determined by substituting $\psi(x)$ into Eq. (30).

Popov (1993) made a rough assumption: $\alpha = (\pi/x_i)^2$, which is obtained by assuming $\psi(x_i) = 0$. As discussed above, $\psi(x_i)$ can not be zero. If so, the temperature at the recombination front is zero rather than T_{ion} . However, the result under this assumption is similar to ours. In our model, α is roughly proportional to x_{ph}^{-2} and x_{ph} decreases with time. Thus the results of Popov (1993) implies the validity of our assumption.

Note that α is time-dependent in our model, which makes $\psi(x)$ also time-dependent. So Eq. (21) should be solved at every time step, when numerical method is implemented.

3. MEDIUM RECOMBINATION APPROXIMATION

Because of the recession of the photosphere, α and $\psi(x)$ varies by the location of photosphere predicted by the Eddington surface boundary condition (Jiang et al. (2022)). We need to determine how the temperature profile responds to the receding photosphere. Assuming the recombination wave as the photosphere, two approximations to the relaxation time of the temperature profile wave were studied by Arnett (1996) (fast and slow approximations). If the recombination front moves slowly, photon diffusion inside the envelope will ensure the temperature profile adjusts to its new outer boundary with the same spatial profile (Popov 1993). While for a fast-moving recombination font, the temperature profile inside will not react to the fact that the out part are being chopped off (Arnett & Fu 1989; Nagy et al. 2014). Generally, the actual response of the temperature to the receding boundary is uncertain. Because Eddington boundary condition may be inaccurate when envelope is optically thin (Fukue 2014). The real evolution of radial temperature profile should be between the slow and fast situations. Therefore, we define a parameter γ to adjust the value of α in each time iteration and fit with observation to obtain the value of γ . The explicit form is written as

$$\alpha_{(\text{cor})}^{i+1} = \alpha^i + \left(\alpha_{(\text{pre})}^{i+1} - \alpha^i \right) \gamma, \quad (31)$$

where $\alpha_{(\text{pre})}^{i+1}$ is calculated from Eq. (30). This is like the predictor-corrector methods in the numerical analysis. The parameter γ is used to adjust the evolution of α to fit observations. Since explosion velocity v_{sc} can be obtained from observation. Substituting v_{sc} into our model and fitting the observed light curve, we obtain the value of γ . $\gamma > 1$ represents α evolves faster than the speed under the current time step. $1 > \gamma > 0$ represents α evolved slower than the current time step. $\gamma = 0$ represents the constant α case, i.e., fast recombination approximation.

The slow recombination approximation assumes the temperature profile evolves with photosphere recession without delay, while the fast one assumes a stationary spatial temperature distribution. They are two limit conditions corresponding to $\gamma = \infty$ and $\gamma = 0$. Because γ is finite, we name our model the medium recombination approximation.

We also find that without the constrain of γ , the evolution of α is related to the time steps in the numerical algorithm. There are two reasons. Firstly, the Eddington approximation may not be accurate at optically thin condition as Fukue (2014) and Choi et al. (2018) suggested. Secondly, both the photosphere and the recombination front are related to the radial temperature profile, i.e. the value of α . However, the value of α is not determined either. One more parameter is required to determine the evolution of α . It can be time step¹ or the γ . The evolution of radial temperature profile is unique for any source. For any given time step, we are always able to adjust γ to get same evolution of $\alpha(t)$, which makes $\alpha(t)$ independent of numerical method. Popov (1993) used luminosity to determine the radius of recombination front. This method is originally proposed in Imshennik & Popov (1992). However, this way is so rough that can only reflect the scaling relation rather than strictly fit observation. One more parameter t_i is needed which determines the moment that recombination starts. In our model, time step and γ also influence that moment, i.e., the value of t_i . Therefore, they are similar way. But our method can fit observation better.

Considering that both the time-step of the numerical method and γ effect the generated light curves, we fix the time step of all the runs in this paper to be $dt = 0.25$ day except for the high resolution runs. In this way, we are able to compare the relative values of γ for different sources.

¹ The time step must be small enough to avoid numerical error. In this paper, 0.25 days is usually short enough.

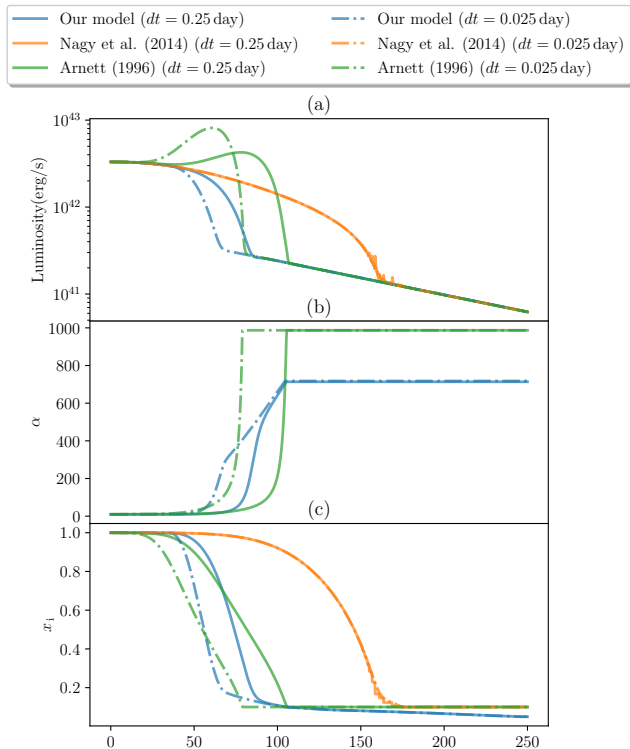


Figure 1. Time evolution of luminosity and the parameters of α and x_i in three models. The blue lines are generated our model; the green lines are from the slow recombination model in Arnett (1996); the orange lines are generated from the model of Nagy et al. (2014). We adopt $\gamma = 1$ in our model.

4. MODEL COMPARISON WITH PREVIOUS WORKS

4.1. Comparison with Arnett (1996) and Nagy et al. (2014)

In Fig.1, we use the same parameters of $R_0 = 5 \times 10^{13}$ cm, $E_{\text{Th}}^0 = E_{\text{kin}} = 0.955 \times 10^{51}$ erg, $\kappa_t = 0.3$ cm²/g, $T_{\text{ion}} = 6000$ K, $M_{\text{Ni}} = 0.04 M_{\odot}$, $M_{\text{ej}} = 10 M_{\odot}$, $A = 0$, $\gamma = 1$ and the numerical time step of $dt = 0.25$ day to compare our results with that of Arnett (1996) and Nagy et al. (2014). We exclude the recombination heat in the three models. We use the slow approximation with $\psi(x) = \sin(\pi x/x_i)/(\pi x/x_i)$ for the model of Arnett (1996). In Fig. 1, we show the results from the three models with two different time steps of 0.25 day and 0.025 day. We observe that α increases significantly during the recession of the photosphere, which also leads to significant change of $\psi(x)$ and $\phi(t)$ (Jiang et al. 2022). The evolution of photosphere is crucial to determine the luminosity.

There is a typo in the equation of A41 in Arnett & Fu (1989), which is corrected in Arnett (1996). Nagy et al. (2014) still adopted the original version, which is

written as:

$$\frac{d\phi(t)}{dt} = \frac{R(t)}{R_0 x_i^3} \left[p_1 \zeta(t) - x_i \frac{\phi(t)}{\tau_d} - 2x_i^2 \phi(t) \frac{R_0}{R(t)} \frac{dx_i}{dt} \right], \quad (32)$$

where p_1 is defined in Eq. (24). From the assumption of Eq. (26) made by Arnett & Fu (1989), the coefficient of the third term in the square bracket of Eq. (32) should be 3, i.e., $3x_i^2 \phi(t) \frac{R_0}{R(t)} \frac{dx_i}{dt}$.

The approximations of Eq. (26) and Eq. (27) on $\psi(x)$ generate an initial bump in luminosity as shown in the green lightcurves in Fig. 1(a). The lightcurves of Fig. 13.12, 13.13, and 13.14 in Arnett (1996) also show similar bumps. The two assumptions about $\psi(x)$ (Eq. (27) and (26)) overestimate dx_i/dt , which make the recombination proceed faster. Arnett (1996) did not consider the evolution of τ_d but simply used a constant τ_d (see Eq. 13.39 in Arnett (1996)), which resulted in a longer plateau phase than our model.

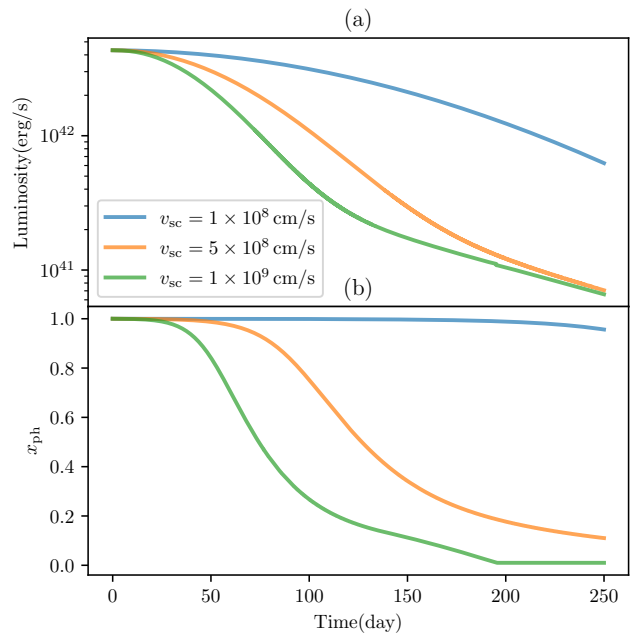


Figure 2. Light curves (panel (a)) and evolution of the photosphere (panel (b)) of our model using the fast recombination approximation. The parameters are the same as in Fig. 1. Different colors indicates different explosion velocities. The blue, orange, and green lines represents the case with $v_{\text{sc}} = 1 \times 10^8$, 5×10^8 , and 1×10^9 cm/s.

By defining I_{ph} , we numerically calculate the integration and derivative of $\psi(x)$ without any approximations (see Eq. (24)). As long as the temperature profile evolves with the recession of the photosphere, we have time-variant α . Along with the updated version of $d\phi(t)/dt$, we generate the light curves of typical SNe IIP. A nat-

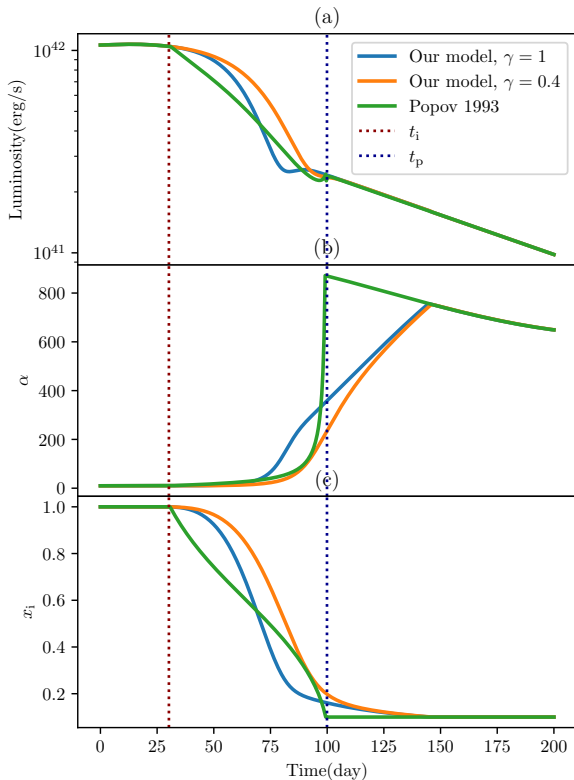


Figure 3. Luminosity and parameter evolution of our model and Popov (1993). The blue and orange lines come from our model with $\gamma = 1$ and 0.4 respectively; the green line is the result from Popov (1993). The time steps of all the models are 0.25 day. The recombination begins at t_i and stops at t_p , which are marked with red and blue dotted lines in the figure.

ural question is, does Eq. 24 still work under the fast approximation? We present the light curves calculated by our model with a constant α ($\gamma = 0$) and different initial kinetic energies in Fig. 2, which are obviously different from SNe IIP. Therefore we conclude that the coevolution of α and boundary condition is essential for modeling the lightcurves of SNe IIP.

4.2. Comparison with Popov (1993)

Popov (1993) proposed that the luminosity given by diffusion approximation equals to the black body radiation of the photosphere (See Eq. (11) in their paper). In this way, the temperature profile parameter α does not influence the position of the recombination front, which makes the model not affected by the time step. However, this approach requires another input parameter t_i for calculation, which is hard to obtain accurately. The an-

alytical expression of the position of pseudo-photosphere (x_i) is expressed as

$$x_i^2(t) = \frac{t_i}{t} \left(1 + \frac{t_i^2}{3t_a^2} \right) - \frac{t^2}{3t_a^2}. \quad (33)$$

where t_i is the moment when the recombination begins and t_a is a character time related to the diffusion and expansion time. In Fig. 3², we compare our results with Popov (1993) by using their parameters of $E = 10^{51}$ erg, $R_0 = 500 R_\odot$, $M_{ej} = 10 M_\odot$, $\kappa = 0.34$, $t_i \approx t_a/\sqrt{\Lambda} = 30.2$ day. The recombination wave defined in Popov (1993) propagates slower than our model, giving lower slope in the light curve during the transition phase. Two different γ values are implemented in Fig. 3, $\gamma = 0.4$ agrees with Popov (1993) better. Although the propagation of recombination wave in Popov (1993) is not influenced by numerical time step, a new parameter t_i is introduced in their work, which has similar effect as γ in our model. Both of them controls the duration of the plateau phase.

4.3. Comparison with SNEC

SNEC solves the hydrodynamics and diffusion radiation transport in the expanding envelopes of core-collapse supernovae, taking recombination effects and the decay of radioactive nickel into account. We compare our results with that of SNEC, which is presented in Fig. 4. Our model star is a red supergiant whose internal structure is derived from a $15 M_\odot$ zero-age main sequence star obtained from the 1D stellar evolution code MESA (Paxton et al. 2013). The evolution of the model star was calculated by MESA. The subsequent hydrodynamic evolutions were followed by SNEC. The SNEC simulation is set up with a thermal bomb with an initial condition of: model mass $M = 12.29 M_\odot$, initial radius $R_0 = 1038.71 R_\odot$, nickel mass $M_{Ni} = 0.04 M_\odot$, and total energy $E_{tot} = 10^{51}$ erg. The lower model mass in the initial condition for the explosion is due to the mass loss during MESA simulation. SNEC code calculates opacity in each grid point of the model from the existing Rosseland mean opacities for different components, temperature and densities of matter. The floor value for opacity needs to be determined. Using the default set up of SNEC code, we set the opacity floor in the envelope (solar metallicity $Z_\odot = 0.02$) to be $0.01 \text{ cm}^2/\text{g}$ and core ($Z = 1$) to be $0.24 \text{ cm}^2/\text{g}$ (Bersten et al. 2011), which is also adopted in Nagy & Vinkó (2016). Following Nagy & Vinkó (2016), we set the opacity in our semi-analytical model to be $0.24 \text{ cm}^2/\text{g}$.

² The calculation of light curves in this figure does not include recombination heat and gamma-ray leakage.

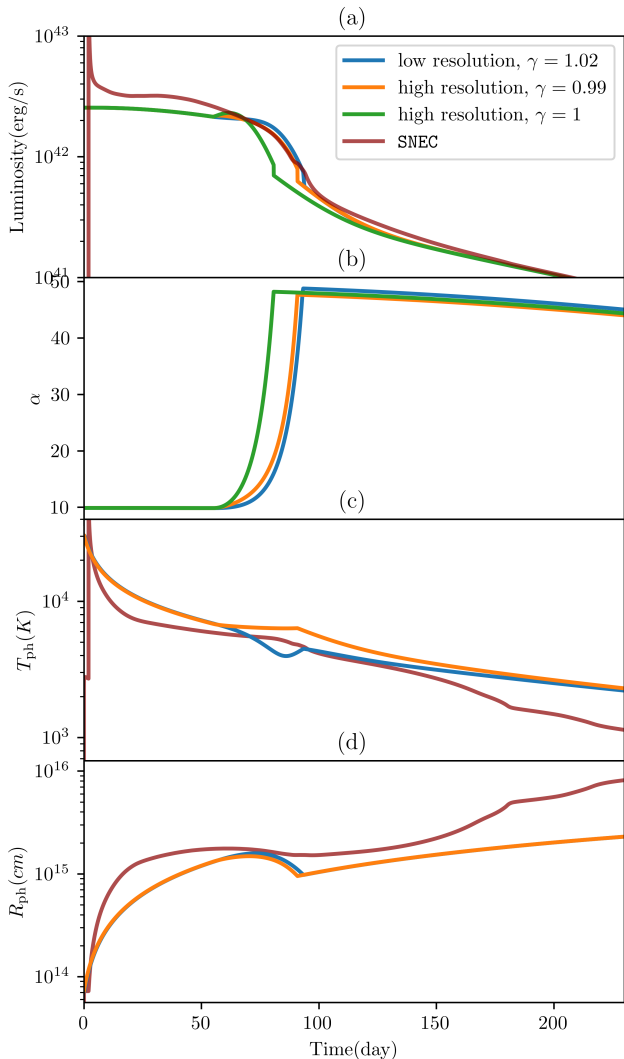


Figure 4. A comparison between the results from our semi-analytical model and that from the hydrodynamic simulations of SNEC. The time step for the low resolution run is 0.25 day, and the high resolution run is 0.025 day.

For the initial condition of our numerical calculations, we adopt the same ejecta mass M_{ej} , initial radius R_0 , Nickel mass M_{Ni} , and total energy E_{tot} as in SNEC simulations. The time step used in Fig. 4 is $dt = 0.25$ day for low resolution run, and $dt = 0.025$ day for the high resolution run. As the blue and orange lines show in Fig. 4, both the high and low resolution runs of our model matches the numerical result well. As discussed in Sec. 3, the evolution of $\alpha(t)$ determines the length of plateau phase, which is adjusted by γ . For the different time step runs in Fig. 4 (blue and orange lines), different values of γ are chosen to match the numerical result. Although the values of γ are different, the evolution of $\alpha(t)$ and the light curves are almost the same.

5. THE EFFECTS OF DIFFERENT PARAMETERS

In Fig. 5, light curves with different initial conditions are plotted. In each panel, the orange line represents our fiducial run which shares the same initial parameters as in Fig. 1. The time step of all the models in this section is $dt = 0.25$ day, as the same in previous sections.

The light curves from SNe IIP with different ejecta masses are presented in Fig. 5(a). Although other parameters are the same, the SN ejecta with smaller initial radius has significantly lower luminosity during plateau phase. This result roughly agree with Stefan–Boltzmann law.

Fig. 5(b) represents the effect of different ejecta mass. Longer cooling time is required for the ejecta with higher mass, which leads to a longer plateau phase. The denser envelope makes slower photosphere recession is also responsible for the longer plateau phase for the higher ejecta mass. On the other hand, ejecta mass also has minor effect to the slope during the transition phase.

Fig. 5(c) shows the effect of different explosion energies from the SNe under the assumption of equal kinetic energy and thermal energy. In general, lengths of the plateau phases of the SNe here are close, but luminosities are different. High explosion energy generates higher effective temperature and faster expanding. However, high expanding velocity causes high cooling rate which leads to shorter plateau phase. Thermal energy and kinetic energy compensate with each other. The difference of the plateau phase is hard to be too large. Main effect of the SN energy is the plateau luminosity.

The effectiveness of gamma-ray trapping A_g mainly influence the slope of radioactive tail (see Fig. 5(d)). For the typical time scale of a supernova $t_{\text{scale}} \sim 300$ day, when A_g is higher than $\sim 10^5 \text{ day}^2$, we are safe to assume all the gamma ray is trapped. For the effect of the radioactive decay of ^{56}Ni , our model shows similar result with Nagy et al. (2014). Thus it is not presented in Fig. 5

To avoid negative value for the recombination front x_i , a minimum value x_0 for it is required. The physical meaning of it is that it corresponds to the boundary of the inner high dense and temperature core of the supernova. The effect of different x_0 is presented in Fig. 5(e). During the transition phase, it primarily affects the ending moment of the rapid decrease of luminosity. When $x_0 \lesssim 0.2$, the effect from this parameter is negligible.

In Fig. 5(f), the light curves from different opacity is plotted. Low opacity model generates higher plateau phase. The lengths of the plateau phases from different opacity are basically similar.

The effect of different density distributions is presented in Fig. 5(g). Different exponential index A in

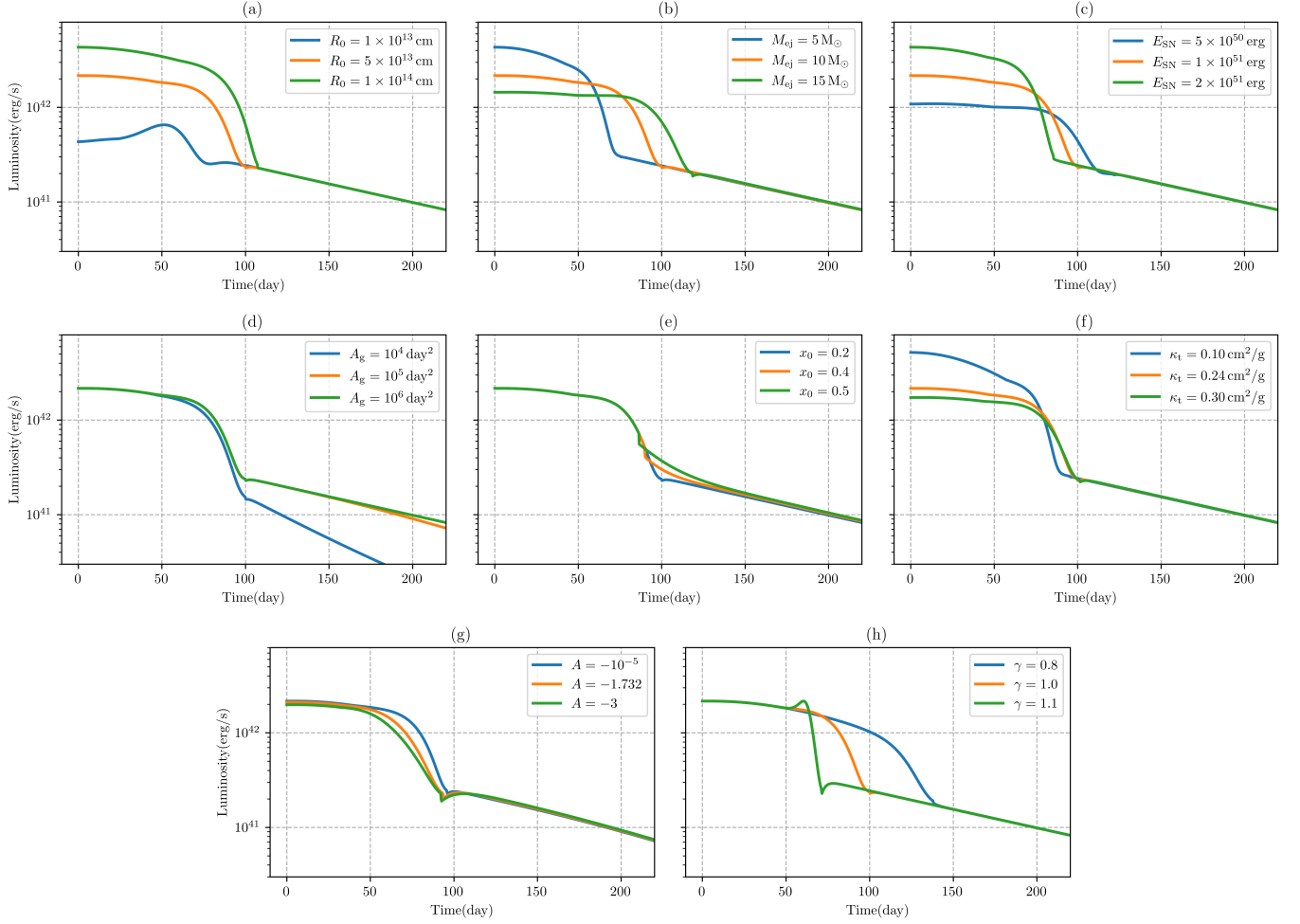


Figure 5. In each panel, we investigate the impact of one single parameter on our model by varying its value while keeping all other parameters constant. The fiducial model is represented by the orange line in all panels, which shares the same parameter values as depicted in Fig. 1. The other two light curves show the effect of changing one parameter at a time. The investigated parameters are: (a) initial radius of envelope R_0 ; (b) ejecta mass M_{ej} ; (c) explosion energy E_{SN} ; (d) gamma-ray trapping effectiveness A_g ; (e) minimum recombination front x_0 ; (f) opacity κ_t ; (g) exponential index of density distribution A ; (h) dimensionless index γ .

$\eta(x)$ has relatively weak effect to the morphology of the light curve. The slope of the radial density distribution mainly affects the slope of the light curves during transition phase.

The effect of γ and explosion velocity (E_{kin}), shows similar effect to the light curves. As Fig. 5(h) shows, different γ value makes different length of plateau phase, which is similar with the effect of explosion velocity (see Fig. 3a in Nagy et al. (2014)). The higher γ or explosion velocity, the shorter generated plateau phase. The physics behind kinetic energy and γ also has some similarity. The expansion of the envelope decreases the temperature inside it. While γ implies the cooling rate of the envelope, higher γ also leads to lower temperature. That is why both E_{kin} and γ influence the length of the plateau. Moreover, initial thermal energy E_{Th}^0 (Nagy

et al. 2014) and initial radius R_0 also have almost the same effect to the light curve. The degeneracy of the parameters has been found in Goldberg (2019). To accurately determine the exact value of these parameters when fitting to a specific source, we manually input the explosion velocity v_{sc} into the model, and assume initial thermal energy equals kinetic energy ($E_{\text{Th}}^0 = E_{\text{kin}}$). Define the energy of the supernova is $E_{\text{tot}} = E_{\text{kin}} + E_{\text{Th}}^0$, in which gravitational energy is neglected. We have 6 parameters to determine the light curves, which are total energy E_{tot} , ejecta mass M_{ej} , mass of ^{56}Ni M_{Ni} , initial radius R_0 , dimensionless parameter γ and density distribution parameter A if necessary. For most cases, we only use M_{Ni} , M_{ej} , γ and R_0 as free parameters to fit, while total energy E_{tot} is partially given by observation (Only M_{ej} is unknown).

6. TWO-COMPONENT MODEL

A two-component model is proposed in [Nagy & Vinkó \(2016\)](#) to explain the initial spike in the light curves of type-IIP supernovae. The density profile of the envelope is assumed to follow the broken power law, which has been widely adopted ([Chevalier 1982](#); [Matzner & McKee 1999](#); [Kasen & Bildsten 2010](#); [Moriya et al. 2013](#)). In previous sections, we are focusing on the core part of the envelope. As suggested in [Nagy & Vinkó \(2016\)](#), the sparse shell component is essential for the initial spike at very early epoch. We adopt a broken power law density profile for the shell component as follows:

$$\eta(x) = \begin{cases} (x/x_0)^{-\delta} & 0 \leq x \leq x_0, \\ (x/x_0)^{-n} & x_0 \leq x \leq 1, \end{cases} \quad (34)$$

where δ is usually assumed to be zero ([Liu et al. 2018](#); [Nagy & Vinkó 2016](#)), n is a free parameter to fit. For $n \sim 10$ is the SN Ib/Ic and SN Ia progenitors ([Liu et al. 2018](#); [Matzner & McKee 1999](#); [Kasen & Bildsten 2010](#); [Moriya et al. 2013](#)). The photosphere x_{ph} in this case see [Jiang et al. \(2022\)](#). For a normal type IIP supernova, its light curve has three main components, i.e., the initial spike, plateau, and radioactive decay tail. The latter two are modeled with exponential/uniform density profiles in previous sections. For the initial spike, the light curve of a sparse shell is needed. The total luminosity of the two components produces the light curves of type IIP supernovae.

As shown in our previous work ([Jiang et al. 2022](#)), the light curve of the broken power law density profile with index $n = 10$ has a minimal temperature gradient, which makes the effect of photosphere recession negligible. This work considers both the photosphere recession and recombination into both components of the model. In the core region, the recombination front and photosphere are very close, which makes the recombination front can be treated as pseudo-photosphere. However, in the shell region, the photosphere recedes deep in the shell ($x_{\text{ph}} \sim 0.2$) before recombination starts. It's incorrect to set the recombination front as photosphere in this case. If so, before recombination starts (within 15 days after explosion), the recombination front is the edge of the ejecta, whose speed is precisely the speed of the edge of the envelope v_{sc} . While the envelope is expanding, there is slight deceleration, which makes v_{sc} can be approximated as a constant. Since observation in [Zhang et al. \(2022a\)](#) shows a rapid decrease of photospheric velocity. Thus setting recombination front to be pseudo-photosphere is not appropriate in this case.

7. FITTING WITH OBSERVATION

In this section, we present our model fitting of five sources and comparison of the best fit parameters between our model and former works. For all the runs we assume $\kappa = 0.3 \text{ cm}^2/\text{s}$ for the core component, and time steps dt are all 0.25 day.

7.1. SN 2016gfy

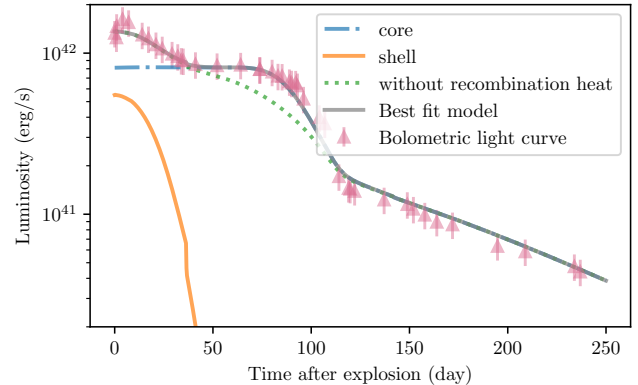


Figure 6. The fitting result of the bolometric light curve of SN 2016gfy. The blue dashed dotted line represents the contribution from core component of our model; orange solid line is the shell component; the green dotted line is the photospheric luminosity without the contribution of recombination heat; the grey solid line is the total luminosity from our model, and the pink error bars are the bolometric data from [Singh et al. \(2019\)](#).

Parameter	Our model		Literature*
	core	shell	
γ	0.77	-	-
$M_{\text{ej}}(M_{\odot})$	13.6	0.5	14.6
$E_{\text{tot}}(10^{51} \text{ erg})$	2.86	-	-
$E_{\text{k}}(10^{51} \text{ erg})$	1.42	0.05	0.9-1.4
$E_{\text{th}}(10^{51} \text{ erg})$	1.42	0.001	-
$M_{\text{Ni}}(M_{\odot})$	0.031	-	0.033 ± 0.003
$R_0(R_{\odot})$	160	503	$\sim 350 - 700$
n	-	4	-

Table 1. Fitting result for SN 2016gfy. * The estimated parameters come from [Singh et al. \(2019\)](#).

We present our light curve fitting with the bolometric luminosity of SN 2016gfy in Fig. 6, and fitting parameters are in Table 1. The bolometric data from SN 2016gfy comes from [Singh et al. \(2019\)](#). The explosion velocity of the core component is 4200 km/s, which is chosen from the speed of Fe II line at the end of plateau phase. Although the effect of Nickel mixing is considered important in [Singh et al. \(2019\)](#), our

model is able to fit the bolometric light curve well without adding this effect. Only from the morphology of the light curve may not enough to demonstrate the importance of Nickel mixing, which requires more detailed study (Nakar 2016). We point out here, the reason why the LC2 (Nagy et al. 2014) does not fit SN 2016gfy well may come from the previously discussed assumptions about $\psi(x)$ from Arnett & Fu (1989) and lacking the effect of photosphere recession (Jiang et al. 2022).

The physical reason that the our model provides relatively flat plateau phase rather than slowly decreasing, comes from the contribution of recombination heat (the second term in Eq. (25)). Since recombination happens outside of photosphere (see Eq. (10) and Liu et al. (2018)). The energy from the Hydrogen recombination is directly added to the total luminosity (Nagy et al. 2014). The red dotted line in Fig. 6 shows the light curve without the recombination heat, which demonstrates the flattened plateau is contributed by recombination heat.

7.2. SN 2019va

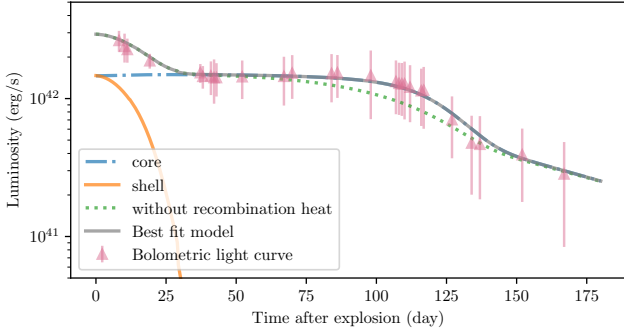


Figure 7. The fitting result for SN 2019va. The lines and dots share the same meaning with that of Fig. 6.

Parameter	Our model		Literature*
	core	shell	
γ	0.87	-	-
$M_{\text{ej}}(M_{\odot})$	19.59	0.3	17.1
$E_{\text{tot}}(10^{51} \text{ erg})$	2.54	-	-
$E_{\text{k}}(10^{51} \text{ erg})$	1.27	0.04	1.15
$E_{\text{th}}(10^{51} \text{ erg})$	1.27	0.001	-
$M_{\text{Ni}}(M_{\odot})$	0.098	-	0.088 ± 0.018
$R_0(R_{\odot})$	466.56	1006.18	289
n	-	4	-

Table 2. Fitting result for SN 2019va. * The estimated parameters come from Zhang et al. (2022a).

The fitting result of SN 2019va is presented in Fig. 7. The bolometric data of SN 2019va comes from Zhang

et al. (2022a). From their work the explosion velocity is ~ 3000 km/s. We choose $v_{\text{sc}} = 3300$ km/s for the calculation of light curve in Fig. 7. The fitting parameters and comparison with the value provided in Zhang et al. (2022a) are presented in Table. 2. The shell component in our result has much larger initial radius than the value provided in Zhang et al. (2022a). The parameters estimated in Zhang et al. (2022a) comes from the empirical relation (Litvinova & Nadezhin 1985) that uses the data at 50 day after the explosion, which can not reflect the information when the outer shell is dominant (less than 30 day after the explosion). Therefore, their result only reflects the size of the core component.

7.3. SN 1999em

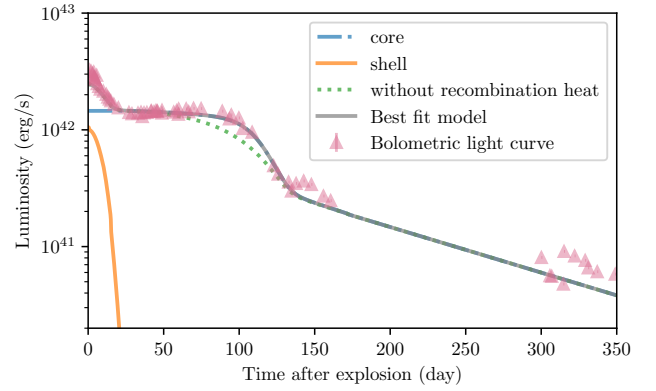


Figure 8. The fitting result for SN 1999em. The lines and dots share the same meaning with that of Fig. 6.

Parameter	Our model		Literature ¹	Literature ²
	core	shell		
γ	0.85	-	-	-
$M_{\text{ej}}(M_{\odot})$	19	0.2	$19.10_{+3.57}^{-6.18}$	$13.16_{+4.94}^{-2.04}$
$E_{\text{tot}}(10^{51} \text{ erg})$	3.27	-	-	-
$E_{\text{k}}(10^{51} \text{ erg})$	1.64	0.01	$4.21_{+4.10}^{-1.55}$	$2.52_{+2.19}^{-0.78}$
$E_{\text{th}}(10^{51} \text{ erg})$	1.64	0.06	$0.32_{+9.98}^{-0.05}$	$3.47_{+4.85}^{-3.21}$
$M_{\text{Ni}}(M_{\odot})$	0.06	-	0.06	0.04
$R_0(R_{\odot})$	350	500	$947.25_{+53.18}^{-918.50}$	$74.74_{+927.12}^{-46.00}$
n	-	6	-	-

Table 3. Fitting result for SN 1999em. Column ¹ and column ² are the two different sets of fitting result in Jäger et al. (2020).

The fitting result for SN 1999em is presented in Fig. 8. The original multiband data comes from Leonard et al. (2001, 2003); Elmhamdi et al. (2003). The bolometric data is from Zhang et al. (2022a), which is obtained using the Superbol package (Nicholl 2018). For

the light curve fitting, we choose the explosion velocity $v_{sc} = 3800$ km/s, which is the photospheric velocity 50 day after the explosion (Elmhamdi et al. 2003). The fitting parameter and comparison with other literature are listed in Fig. 3. In general, our model provide similar parameters with the two different sets in Jäger et al. (2020). The parameters in Jäger et al. (2020) shows large uncertainty about the initial radius of the ejecta. Our result is between the two sets and within the uncertainty.

7.4. SN 2004et

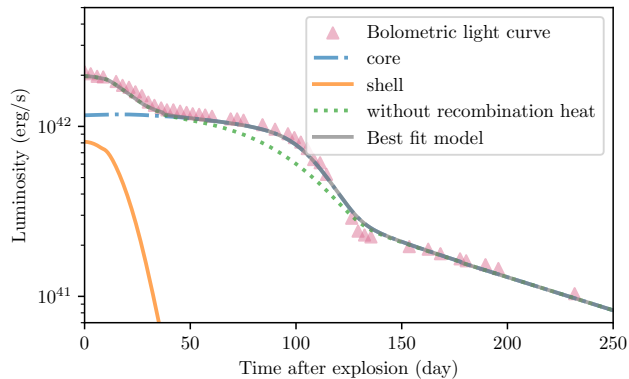


Figure 9. The fitting result for SN 2004et. The lines and dots share the same meaning with that of Fig. 6.

Parameter	Our model		Literature ¹	Literature ²
	core	shell		
γ	0.8	-	-	-
$M_{ej}(M_{\odot})$	12.0	0.8	11.0	14.0
$E_{tot}(10^{51} \text{ erg})$	1.75	-	1.95	0.88
$E_k(10^{51} \text{ erg})$	0.88	0.0006	-	-
$E_{th}(10^{51} \text{ erg})$	0.88	0.07	-	-
$M_{Ni}(M_{\odot})$	0.053	-	0.06	0.036
$R_0(R_{\odot})$	330	480	603.71	631.02
n	-	3	-	-

Table 4. Fitting result for SN 2004et. The fitting parameters from column ¹ are from Nagy et al. (2014) and column ² are from Maguire et al. (2010).

The light curve fitting for SN 2004et is presented in Fig. 9, and fitting parameters and comparison with literature (Nagy et al. 2014; Maguire et al. 2010) are listed in Table. 4. We choose the explosive velocity to be 3500 km/s which is the mid-plateau velocity ~ 3560 km/s in Sahu et al. (2006). The bolometric data is obtained from (Nagy & Vinkó 2016). We observe a

longer shell component compared to other sources in this paper, which accounts for the higher shell mass in our model.

7.5. SN 2005cs

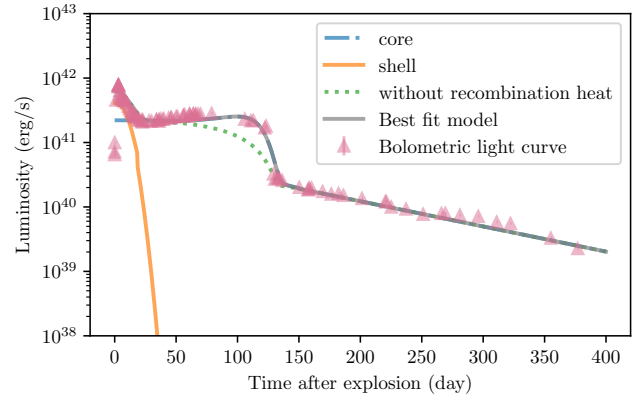


Figure 10. The fitting result for SN 2005cs. The lines and dots share the same meaning with that of Fig. 6.

Parameter	Our model		Literature*
	core	shell	
γ	0.925	-	-
$M_{ej}(M_{\odot})$	8.7	0.3	8.61
$E_{tot}(10^{51} \text{ erg})$	0.32	-	0.3
$E_k(10^{51} \text{ erg})$	0.20	0.025	-
$E_{th}(10^{51} \text{ erg})$	0.12	0.0025	-
$M_{Ni}(M_{\odot})$	0.005	-	0.0018
$R_0(R_{\odot})$	201.24	450	175.36
n	-	4	-

Table 5. Fitting result for SN 2005cs. * The estimated parameters come from Tsvetkov et al. (2006).

We present the light curve fitting in Fig. 10. The fitting parameters as well as comparison with Tsvetkov et al. (2006) are listed in Table 5. The original multi-band data comes from Pastorello et al. (2006, 2009). Similar with SN 1999em, the bolometric data is calculated with Superbol code (Nicholl 2018) and obtained from Zhang et al. (2022a). For this source, the light up at the end of the plateau is relatively larger than other sources. The contribution of recombination heat is higher (the area between the black solid line and red dotted line). The relatively larger M_{Ni} in our model compared with Tsvetkov et al. (2006) is from the unusually low ^{56}Ni in this source, which makes it very sensitive to the luminosity during radioactive tail.

8. DISCUSSION AND CONCLUSION

We integrate a receding photosphere into the previous homologous expansion model and derive the luminosity in a self-consistent way by introducing a medium recombination approximation. We find that the photosphere is strongly related to the recombination front. The recession of the recombination front causes a significant recession of the photosphere. Using the Eddington boundary condition on the photosphere, we find the eigenvalue α is roughly proportional to x_{ph}^{-2} as previous works suggested. At the end of the recombination, α is significantly larger than its initial value. Our medium recombination approximation allows us to determine the model parameters according to the observational data. Moreover, our result is consistent with that of the widely used radiation-hydrodynamic simulations (SNEC).

It is also suggested that magnetars may power the explosions SNe IIP Sukhbold & Thompson (2017); Orellana et al. (2018). In Nagy et al. (2014), the nature of light curves produced by Arnett's analytical model with magnetar powering is briefly investigated. In their work, to get the typical light curves of SNe IIP, the rotational energy of the neutron star must be comparable to the recombination energy. Otherwise, there will not be a plateau in the light curves. This result is consistent with Sukhbold & Thompson (2017), they suggest the strength of the magnetic field should be strong (greater than 10^{15} G), and the rotation period is several milliseconds. Using the relations of the spin-down

time scale and the initial rotational energy of the magnetar, the corresponding scale and the rotational energy in Sukhbold & Thompson (2017) is ~ 0.4 days and $\sim 5 \times 10^{49}$ erg. Applying this result to our model, we found the influence from magnetar can hardly be distinguished. Therefore we do not present a figure with magnetar here. Since the energy injection of the magnetar in both our model and Nagy et al. (2014) are unnecessary. Whether or not SNe IIP are powered by magnetars remains unclear. It still needs more observation in the very early epoch.

Our model can fit light curves of some SNe IIP quite well. For some SNe IIP such as SN 2019va (which is shown in Fig. 6, 7 and 10), their light curve increases mildly at the end of the plateau phase. Zhang et al. (2022a) consider such effect comes from the distribution of ^{56}Ni in the envelope. However, the recombination heat also has a similar effect that lightens up the plateau as discussed in this paper. This puts an alternative channel to explain the flattened and longer plateau other than the Nickel mixing (Kozyreva 2019). We will investigate it in detail in our future work.

ACKNOWLEDGMENTS

We thank Dr. Jozsef Vinko and Dr. Andrea Nagy for providing us their source code. We also thank Dr. Xinghan Zhang for the useful discussion and bolometric data of SN 2019va, SN 1999em and SN 2005cs. We thank Dr. Singh for the bolometric data of SN 2016gfy.

REFERENCES

- Arnett, D. 1996, *Supernovae and Nucleosynthesis*, doi: [10.2307/j.ctv173f2k2](https://doi.org/10.2307/j.ctv173f2k2)
- Arnett, W. D. 1980, *ApJ*, 237, 541, doi: [10.1086/157898](https://doi.org/10.1086/157898)
- . 1982, *ApJ*, 253, 785, doi: [10.1086/159681](https://doi.org/10.1086/159681)
- Valenti, S., Howell, D. H., Stritzinger, M. D., et al. 2016, *MNRAS*, 459, 3939
- Ricks, W., & Dwarkadas, V. V. 2019, *ApJ*, 880, 59
- Goldberg, J. A., Bildsten, L., & Paxton, B. 2019, *ApJ*, 879, 3
- Anderson, J. P., González-Gaitán, S., Hamuy M., et al. 2014, *ApJ*, 786, 67
- Sanders, N. E., Soderberg, A. M., Gezari, S., et al. 2015, *ApJ*, 799, 208
- Utrobin, V. .P., Wongwathanarat, A., H.-Th. Janka, H. T., & Müller, E. 2017, *ApJ*, 846, 37
- Paxton, B., Schwab, J., Bauer, E. B., et al. 2018, *ApJS*, 234, 34
- Paxton, B., Smolec, R., Schwab, J. 2019, *ApJS*, 243,10
- Arnett, W. D., & Fu, A. 1989, *ApJ*, 340, 396, doi: [10.1086/167402](https://doi.org/10.1086/167402)
- Barbon, R., Cappellaro, E., & Turatto, M. 1984, *A&A*, 135, 27
- Chatzopoulos, E., Wheeler, J. C., & Vinko, J. 2012, *Astrophysical Journal*, 746, 121, doi: [10.1088/0004-637X/746/2/121](https://doi.org/10.1088/0004-637X/746/2/121)
- Chevalier, R. A. 1982, *ApJ*, 258, 790, doi: [10.1086/160126](https://doi.org/10.1086/160126)
- Doggett, J. B., & Branch, D. 1985, *AJ*, 90, 2303, doi: [10.1086/113934](https://doi.org/10.1086/113934)
- Eddington, A. S. 1926, *The Internal Constitution of the Stars*
- Jiang, H.-X., Liu, X.-W., & You, Z.-Y. 2022, *ApJ*, 933, 7, doi: [10.3847/1538-4357/ac6f5b](https://doi.org/10.3847/1538-4357/ac6f5b)
- Kasen, D., & Bildsten, L. 2010, *ApJ*, 717, 245, doi: [10.1088/0004-637X/717/1/245](https://doi.org/10.1088/0004-637X/717/1/245)
- Liu, L.-D., Zhang, B., Wang, L.-J., & Dai, Z.-G. 2018, *ApJL*, 868, L24, doi: [10.3847/2041-8213/aaeff6](https://doi.org/10.3847/2041-8213/aaeff6)

- Matzner, C. D., & McKee, C. F. 1999, *ApJ*, 510, 379, doi: [10.1086/306571](https://doi.org/10.1086/306571)
- Rubin, A., et al., 2016, *ApJ*, 820, 33
- Galbany, L., et al., 2016, *AJ*, 151, 33
- Moriya, T. J., Maeda, K., Taddia, F., et al. 2013, *Monthly Notices of the Royal Astronomical Society*, 435, 1520, doi: [10.1093/mnras/stt1392](https://doi.org/10.1093/mnras/stt1392)
- Nagy, A. P., Ordasi, A., Vinkó, J., & Wheeler, J. C. 2014, *Astronomy and Astrophysics*, 571, 77, doi: [10.1051/0004-6361/201424237](https://doi.org/10.1051/0004-6361/201424237)
- Nagy, A. P., & Vinkó, J. 2016, *Astronomy and Astrophysics*, 589, A53, doi: [10.1051/0004-6361/201527931](https://doi.org/10.1051/0004-6361/201527931)
- Popov, D. V. 1993, *ApJ*, 414, 712, doi: [10.1086/173117](https://doi.org/10.1086/173117)
- Kozyreva, A., Nakar, E., & Waldman, R. 2019, *ApJ*, 483, 1211
- Falk, S. W., & Arnett, W. D., 1973, *ApJL*, 180, 65
- Nakar, E., Poznanski, D., & Katz, B., 2016, *ApJ*, 823, 127
- Kasen, D., & Woosley, S. E. 2009, *ApJ*, 703, 2205
- Sukhbold, T., & Thompson, T. A. 2017, *MNRAS*, 472, 224, doi: [10.1093/mnras/stx2004](https://doi.org/10.1093/mnras/stx2004)
- Kou, Shihao., Chen, Xingzhuo., Liu, Xuewen., 2020, *ApJ*, 890, 177
- Faran, T., Poznanski, D., Filippenko, A. V., et al. 2014, *MNRAS*, 442, 844
- Smartt, S. J. 2015, *PASA*, 32, e016, doi: [10.1017/pasa.2015.17](https://doi.org/10.1017/pasa.2015.17)
- Arcavi, I., Gal-Yam, A., Cenko, S. B., et al. 2012, *ApJL*, 756, 30
- Grassberg, E. K., Imshennik, V. S., & Nadyozhin, D. K. 1971, *Astrophysics and Space Science*, 10, 28
- Hiller, D. J., & Dessart., L., 2019, *Astronomy & Astrophysics*, 631, 19
- Zampieri, L., Pastorello, A., Turatto, M., et al. 2003, *MNRAS*, 338, 711, doi: [10.1046/j.1365-8711.2003.06082.x](https://doi.org/10.1046/j.1365-8711.2003.06082.x)
- Dessart, L., Hillier, D. J., Waldman, R., & Livne, E. 2013, *MNRAS*, 433, 1745
- Singh, A., Kumar, B., Moriya, T. J., et al. 2019, *The Astrophysical Journal*, 882, 68, doi: [10.3847/1538-4357/ab3050](https://doi.org/10.3847/1538-4357/ab3050)
- Orellana, M., Bersten, M. C., & Moriya, T. J. 2018, *A&A*, 619, A145, doi: [10.1051/0004-6361/201832661](https://doi.org/10.1051/0004-6361/201832661)
- Zhang, X., Wang, X., Sai, H., et al. 2022a, *MNRAS*, 513, 4556, doi: [10.1093/mnras/stac1166](https://doi.org/10.1093/mnras/stac1166)
- . 2022b, *MNRAS*, 509, 2013, doi: [10.1093/mnras/stab3007](https://doi.org/10.1093/mnras/stab3007)
- Paxton, B., Cantiello, M., Arras, P., et al. 2013, *ApJS*, 208, 4, doi: [10.1088/0067-0049/208/1/4](https://doi.org/10.1088/0067-0049/208/1/4)
- Faran, T., Goldfriend, T., Nakar, E., & Sari, RE. 2019, *ApJ*, 879, 20
- Bersten, M. C., Benvenuto, O., & Hamuy, M. 2011, *ApJ*, 729, 61, doi: [10.1088/0004-637X/729/1/61](https://doi.org/10.1088/0004-637X/729/1/61)
- Jäger, Zoltán, J., Vinkó, J., Bíró, B. I., et al. 2020, *MNRAS*, 496, 3725, doi: [10.1093/mnras/staa1743](https://doi.org/10.1093/mnras/staa1743)
- Maguire, K., Di Carlo, E., Smartt, S. J., et al. 2010, *MNRAS*, 404, 981, doi: [10.1111/j.1365-2966.2010.16332.x](https://doi.org/10.1111/j.1365-2966.2010.16332.x)
- Tsvetkov, D. Y., Volnova, A. A., Shulga, A. P., et al. 2006, *A&A*, 460, 769, doi: [10.1051/0004-6361:20065704](https://doi.org/10.1051/0004-6361:20065704)
- Litvinova, I. Y., & Nadezhin, D. K. 1985, *Soviet Astronomy Letters*, 11, 145
- Leonard, D. C., Filippenko, A. V., Gates, E. L., et al. 2001, *Publications of the Astronomical Society of the Pacific*, 114, 35, doi: [10.1086/324785](https://doi.org/10.1086/324785)
- Leonard, D. C., Kanbur, S. M., Ngeow, C. C., & Tanvir, N. R. 2003, *The Astrophysical Journal*, 594, 247, doi: [10.1086/376831](https://doi.org/10.1086/376831)
- Elmhamdi, A., Danziger, I. J., Chugai, N., et al. 2003, *Monthly Notices of the Royal Astronomical Society*, 338, 939-956, doi: [10.1046/j.1365-8711.2003.06150.x](https://doi.org/10.1046/j.1365-8711.2003.06150.x)
- Nicholl, M. 2018, *Research Notes of the AAS*, 2, 230, doi: [10.3847/2515-5172/aaf799](https://doi.org/10.3847/2515-5172/aaf799)
- Elmhamdi, A., Danziger, I. J., Chugai, N., et al. 2003, *Monthly Notices of the Royal Astronomical Society*, 338, 939-956, doi: [10.1046/j.1365-8711.2003.06150.x](https://doi.org/10.1046/j.1365-8711.2003.06150.x)
- Sahu, D. K., Anupama, G. C., Srividya, S., & Muneer, S. 2006, *Monthly Notices of the Royal Astronomical Society*, 372, 1315-1324, doi: [10.1111/j.1365-2966.2006.10937.x](https://doi.org/10.1111/j.1365-2966.2006.10937.x)
- Pastorello, A., Sauer, D., Taubenberger, S., et al. 2006, *Monthly Notices of the Royal Astronomical Society*, 370, 1752-1762, doi: [10.1111/j.1365-2966.2006.10587.x](https://doi.org/10.1111/j.1365-2966.2006.10587.x)
- Pastorello A., Valenti S., Zampieri L., et al. 2009. SN 2005cs in M51 – II. Complete evolution in the optical and the near-infrared. *Monthly Notices of the Royal Astronomical Society* 394(4):2266-2282. doi: [10.1111/j.1365-2966.2009.14505.x](https://doi.org/10.1111/j.1365-2966.2009.14505.x)
- Fukue, J. 2014, *Publications of the Astronomical Society of Japan*, 66, 1–12
- Choi, J., Dotter, A., Conroy, C., & Ting, Y. S. 2018, *ApJ*, 860, 131
- Imshennik, V. S., & Popov, D. V. 1992, *Astron. Zh.*, 69, 497